Peer-reviewed version available at Water 2018, 10, 775; doi:10.3390/w10060775

Article

Integrated Modeling Approach for the Development of Climate-Informed, Actionable Information

David R. Judi [1,*], Cynthia L. Rakowski [1], Scott R. Waichler [1], and Youcan Feng [1]

[1] Pacific Northwest National Laboratory, Richland, WA 99354, U.S.A.
* Correspondence: david.judi@pnnl.gov

Abstract: Flooding is a prevalent natural disaster with both short and long-term social, economic, and infrastructure impacts. Changes in intensity and frequency of precipitation (including rain, snow, and rain on snow) events create challenges for the planning and management of resilient infrastructure and communities. While there is general acknowledgement that new infrastructure design should account for future climate change, no clear methods or actionable information is available to community planners and designers to ensure resilient design considering an uncertain climate future. This research used climate projections to drive high-resolution hydrology and flood models to evaluate social, economic, and infrastructure resilience for the Snohomish Watershed, WA, U.S.A. The proposed model chain has been calibrated and validated. Based on the established model chain, the peaks of precipitation and streamflows were found to shift from spring and summer to earlier winter season. The nonstationarity of peak discharges was discovered with more frequent and severe flood risks projected. The peak discharges were also projected to decrease for a certain period in the near future, which might be due to the reduced rain-on-snow events. This research was expected to provide a clear method for the incorporation of climate science in flood resilience analysis and to also provide actionable information relative to the frequency and intensity of future precipitation events.

Keywords: climate projections; integrated modeling; flood modeling; nonstationarity

1. Introduction

Extreme flooding has been observed to become more prevalent and is expected to worsen with a changing climate considering the potential for increased precipitation and rain-on-snow events in regions of the United States[1]. Traditional approaches to designing flood mitigation strategies have assumed a stationary climate, but it is increasingly important to consider changes in magnitude and frequency extreme events and include future climate scenarios in design [2].

In many cases, the standards currently used in flood mitigation design using stationary climate assumptions (e.g., historical 100-year return period) are no longer sufficiently conservative assumptions [1]. In recognition of this, there have been recent changes in design standards and floodplain management policy which call for the "consideration" of possible changes induced by climate change [3]. For example, in 2015 a U.S. Presidential Executive Order (13690) mandated changes in the federal flood risk management standard. This order gave agencies the flexibility to either 1) use data and methods informed by best-available, actionable climate science, 2) build two feet above the 100-year flood elevation for standard projects or three feet above for critical buildings, or 3) build to the 500-year flood elevation. Specific guidance on appropriate methods informed by best-available, actionable climate science is not available. Moreover, blindly raising infrastructure by a defined, uniform threshold does not adequately consider risk and may result in either over or under designed mitigation. Approaches that explicitly consider future climate scenarios are needed in order to adequately understand flood risk and develop actionable, climate-informed information at a local scale.

One of the primary challenges in developing local-scale, actionable information for future flood risk is related to the temporal and spatial scales of available climate information. To translate climate projections into local-scale flood prediction, multi-modal approaches connecting general circulation models (GCMs), downscaling methods, hydrological modeling, and consequence analysis present an approach to overcome temporal and spatial resolution challenges [4, 5]. In a multi-model, multi-scale approach, a GCM depicts climate variables at a global scale typically with a spatial resolution of multiple degrees and a monthly temporal scale. These spatial and temporal scales are very coarse compared to that of the watershed-scale hydrological processes [6] and therefore inadequate to use alone in understanding the impacts of climate on flood risk management. To represent watershed-scale processes, Regional Climate Models (RCM) dynamically downscaled to a specific region can be developed by utilizing GCM as boundary conditions for higher resolution, regional climate simulations. This approach in developing RCMs parameterizes physical atmospheric processes and accounts orographic effects and mesoscale processes [7, 8].

GCMs can also be downscaled through statistical approaches are based on relationships in large-scale climate and regional characteristics identified from observational data [6]. Because these approaches do not have a significant computational burden, they are often the method of choice for downscaling. The method of "change factors", also known as the perturbation or the delta-change method, is a simple example of statistical downscaling, which applies the difference in GCM projections between the control and future periods to match the baseline observations [8]. Due to its simplicity, this method is widely used by hydrologists [9, 10]. Another simple statistical method is bias correction, which defines a transfer function for GCM/RCM outputs for the control period to match certain statistical properties of the observations [11]. These simple statistical downscaling approaches have a number of caveats, including assuming a stationary bias through time and a constant spatial pattern of climate [8, 11]. To overcome limitations of both dynamical and statistical downscaling methods, statistical-dynamical processes can be used to further remove inherent bias [12].

At the watershed scale, hydrologic models ingest climatic variables such as temperature, precipitation, and humidity derived from downscaled GCMs/RCMs to simulate hydrologic processes and ultimately provide a continuous estimate of river discharges. Calibration of hydrologic models is important in order to reduce the uncertainty in the flow estimates, especially for watersheds sensitive to pronounced seasonal changes (e.g., rain and snow interactions) [13-15]. Statistical distributions of extreme river discharge events can be developed using the continuous estimates of river discharge [16].

To develop actionable flood risk information, thresholds from the statistical distribution of river flows can be developed and used to drive high-resolution flood extent estimation. Various approaches exist to estimate flood extent, including empirical, hydrodynamic, and non-physics-based models [17], but is an essential component in assessing infrastructure exposure to floods and subsequent damage estimates. Ensembles of flood extents and associated damage estimates derived from sampling the statistical river flow distribution are foundational to robust probabilistic risk [18].

The objective of this research is to develop an end-to-end, multi-scale, multi-model framework to effectively integrate GCM/RCM, hydrology, and flood risk to develop local-scale, actionable information to be used in flood management. These tools will provide a means to develop mitigation and adaptation strategies to ensure resilient designs of communities and critical infrastructure systems. The achieved actionable information will help local stakeholders (including policy makers, planners, and engineers) understand vulnerabilities and consequences related to the nonstationarity of precipitation events.

2. Method

To overcome spatial and temporal resolution challenges and incorporate climate nonstationarity into flood risk management, a multi-scale, multi-model flood risk framework has been developed (Figure 1). This framework is intended to provide a means to develop quantifiable and actionable flood risk information at a local scale.

Preprints (www.preprints.org) | NOT PEER-REVIEWED | Posted: 2 May 2018 doi:10.20944/preprints201805.0044.v1

Peer-reviewed version available at Water 2018, 10, 775; doi:10.3390/w10060775

The framework is presented in the context of a case study based on the Snohomish River Basin located near Monroe, WA (Figure 2**Error! Reference source not found.**). This river basin is of particular interest for this case study because of the river peak flows sensitive to rain, snow, and rain-on-snow events. The basin has frequent fluvial flooding, with overtopping expected to happen every 2 to 5 years [19]. The Snohomish River Basin belongs to the U.S. Pacific Northwest region, which was projected to experience the temporal and spatial changes in precipitation, with possible shifts of flood and low flow extremes [20].

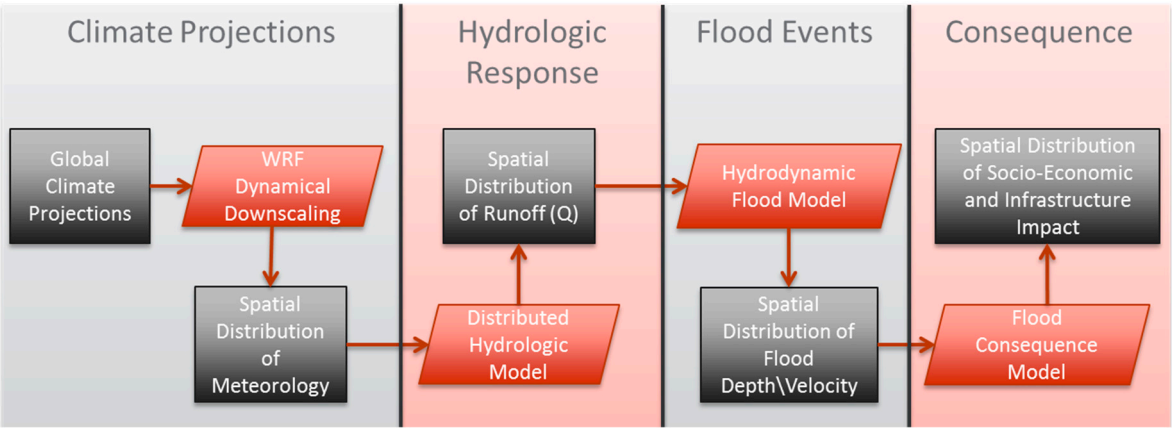

Figure 1. Integrated multi-scale, multi-model framework for flood risk estimation

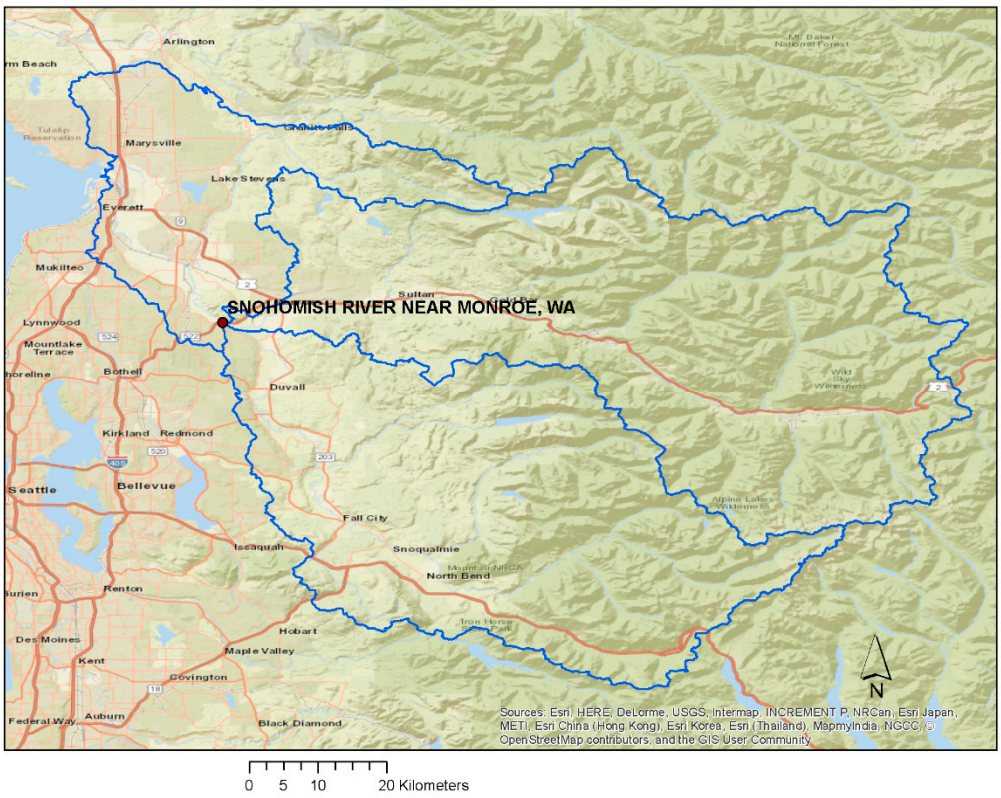

Figure 2. The Snohomish watershed (blue lines) and the location of the USGS gauge near Monroe, WA.

2.1. Climate Modeling and Downscaling

Existing climate datasets from the Platform for Regional Integrated Modeling and Analysis (PRIMA) were extracted for the Snohomish basin [21, 22], where the GCM output was downscaled using the Weather Research and Forecasting (WRF) model [23] with specific emphasis on the Pacific Northwest. These dynamically downscaled climate simulations were then bias corrected to match the North American Land Data Assimilation (NLDAS-2) monthly data [24] as mentioned in Hejazi et al [25] using the Bias-Correction Spatial Disaggregation (BCSD) method described by Wood et al [5]. Bias correction was applied to precipitation and temperature, respectively. For temperature, the linear trend was removed and then the quantile mapping was used. For precipitation, however, there was no linear trend to remove, so quantile mapping was applied to both the historic and future periods. Downscaled precipitation was compared to the U.S. National Oceanic and Atmospheric Administration (NOAA)'s Global Historical Climatology Network-Daily (GHCN-D) database which provides the observed precipitation records. Seven sites were selected for having sufficient length of record and representative locations and elevations within the watershed (Table 1).

Table 1. NOAA Daily Precipitation Sites. Only calendar years with at least 300 recorded days were included in the analysis.

Station	Elevation	Water Years	Total of Years
Baring (47.7722°N, 121.4819°W)	235m	1978-1998, 2000, 2002-2003	24
Everett (47.9753°N, 122.1950°W)	18m	1978-2003	26
Monroe (47.8453°N, 121.9944°W)	37m	1978-2003	26
Snoqualmie Falls (47.5414°N, 121.8361°W)	134m	1978-1995, 1997-2003	25
Startup (47.8664°N, 121.7175°W)	52m	1978-2003	26
Stevens Pass (47.7372°N, 121.0914°W)	1241m	1978-1980, 1995-1997, 1999, 2000	8
Tolt S. Fork Reservoir (47.7000°N, 121.6908°W)	610m	1978-1984, 1986-1988, 1990-1991, 1993, 1995-2000, 2002-2003	21

The RCM includes three groups of climate datasets used to bound the study- historical simulated data (hereafter referred to as historic), and Representative Concentration Pathway 4.5 (RCP4.5) and 8.5 (RCP8.5). The historic data is representative of water years 1978 to 2003 and the RCP scenarios represent future time periods (water years: 2022 to 2100). For this study, the future periods were further decomposed into two separate time periods- 2022 to 2055 and 2067 to 2100. The RCM data consisted of hourly data for air temperature, wind speed, relative humidity, incoming shortwave radiation, longwave radiation, and precipitation. These hourly data were aggregated to the 3-hourly format for use by the hydrologic model.

2.2. Hydrologic Modeling

To translate regional climate data into local-scale runoff distributions, the Distributed Hydrology Soil Vegetation Model (DHSVM) [26] was used to simulate the hydrological processes including precipitation, infiltration, snow accumulation and melt, and runoff at a 3-hourly timescale. The DHSVM model was established for the Snohomish basin at 150-m resolution using the previously described meteorological forcing data [27].

DHSVM was further calibrated by adjusting parameters including temperature thresholds impacting rain, snow, and rain-on-snow transitions. In addition, lateral conductivity was used as a calibration parameter, initially set using published values related to specific soil layers [28] and subsequently uniformly adapted through calibration. Both the temperature thresholds and the lateral conductivity affect the timing and volume of peak runoff.

To optimize the hydrologic calibration process, the Multi-objective Complex Evolution Model (MOCOM) [29] was used to fully explore the parameter space and optimize the parameters via an objective function through successive generations of parameters. The objective function for calibration was maximizing fit relative to extreme runoff events, where fit was measured as a function of the coefficient of determination (R^2), Nash-Sutcliffe Efficiency (NSE), and the root-mean-square error (RMSE) based on the work of Moriasi et al [30]. The DHSVM calibration and validation period, each a 10-year period, was driven by meteorological observations available in the NLDAS-2 dataset (Figure 3). The calibration and validation point was at a USGS stream gage locations (ID: 12150800 Snohomish River near Monroe, WA, U.S.A.) near the downstream end of the basin. The calibrated and validated DHSVM model was rerun using the RCM historic, RCP4.5, and RCP8.5 meteorological forcings under the time periods shown in Table 2.

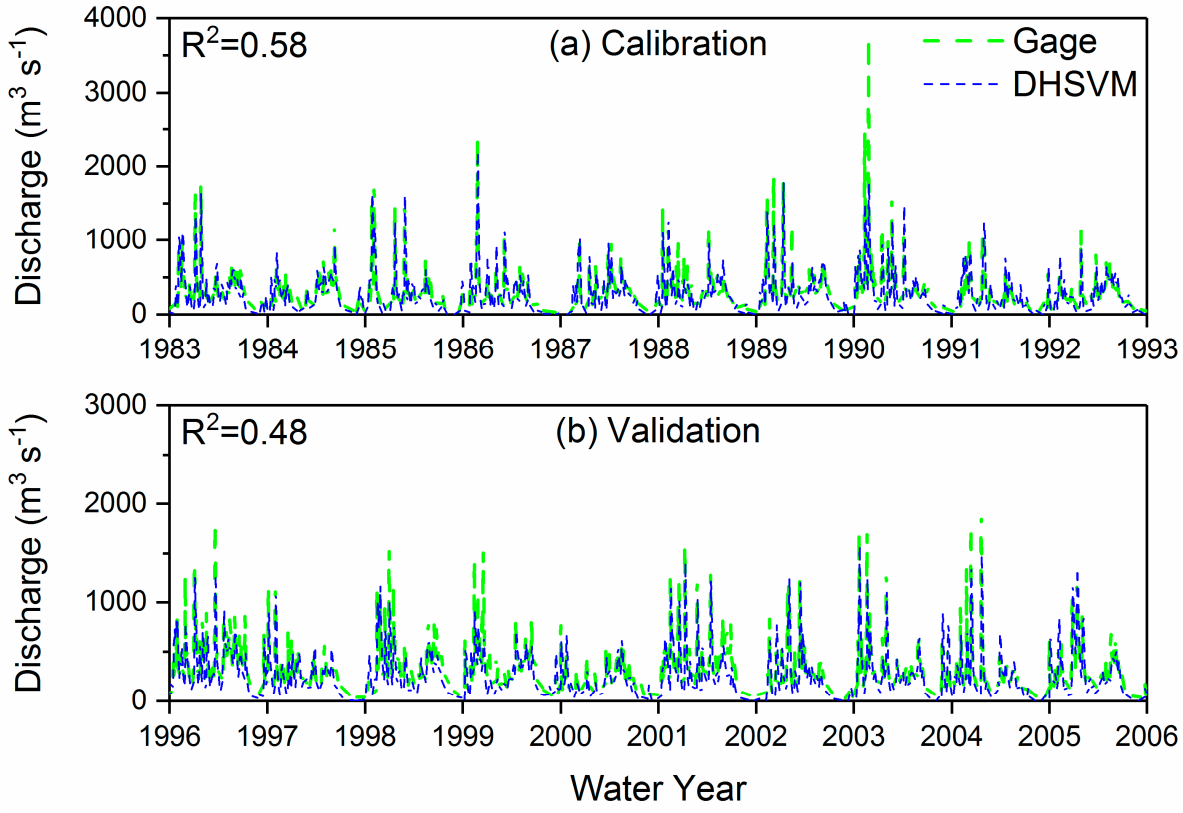

Figure 3. DHSVM calibration and validation at Monroe, WA.

Table 2. Water years used for flow frequency analysis.

Scenarios	Years
USGS	1964-2015
Historic	1978-2003
RPC4.5	2022-2055, 2067-2100
RPC8.5	2022-2055, 2067-2100

2.3. Frequency Analysis

The hydrologic simulations produce a continuous distribution of flows over the duration of the study period. To be able to change relative to flood risk, methods are needed to develop statistical distributions of annual extreme events consistent with engineering design criteria. To this end, the Bulletin 17C method [31] was used to develop statistical extreme event distributions derived from the streamflow simulations generated by DHSVM.

There are significant uncertainties in developing future realizations of flood risk with contributions from multiple aspects of the multi-scale, multi-model process [6, 32-37]. For example, while climate models generally do well at representing decadal variability, and to some extent, monthly variability, and representation of annual extremes is challenging.[38-41]. The inability to capture extremes in the meteorological variables translates to an inability to capture extremes in runoff and subsequently an underestimation in statistical distributions of annual extreme events. Because the climate inputs for the Historic and RCP simulations share the same biases and uncertainties, we employ a post frequency analysis bias correction based on differences between the historic simulated data and observed USGS extreme event statistical distributions:

$$\boldsymbol{PFrcp'_p = PFusgs_p + (PFrcp_p - PFhistoric_p)}, \quad (1)$$

where $PFrcp'_p$ is the bias-corrected annual extreme flow of an RCP scenario for a given return period event, p; $PFusgs_p$is the annual extreme flow of the derived from USGS instantaneous annual peak flow for a given return period event, p; $PFrcp_p$ is the annual extreme flow of an RCP scenario for a given return period event, p, and $PFhistoric_p$ is the peak flow of the historic simulated period for a given return period event, p.

2.4. Hydrodynamic and Consequence Modeling

Statistical distributions representing the change in annual extreme events are not sufficient in developing local-scale, actionable information. To be effective and capture the nonlinearity that exists in flood risk analysis, the statistical distributions of annual extreme flow rates must be translated to spatial estimates of flood extents. To capture the flood extent, a two-dimensional hydrodynamic model based on the shallow water equations is used to characterize extreme event flood behavior. [42]. This model utilizes best-available topographic data and does not require prior knowledge of flow path, effectively able to capture floodplain dynamics.

To develop spatial probabilistic risk estimates and capture changes from historic to future climate, samples are taken from across the distributions of extreme events. In this study, nearly 140 samples from each statistical distribution (observed and both RCP projections) were taken and each sample was used to drive a hydrodynamic simulation and develop corresponding spatial estimates of flooding. For each hydrodynamic simulation, inundation depths were used to estimate the flood damage and annualized flood risk based on depth-damage fragility curves available from HAZUS-MH [43]. The direct damage can be determined by intersecting the depth from the depth-damage curves to retrieve the percent damage:

$$\boldsymbol{D = \sum_{g=1}^{n}(fc_{g,h} \times SV_g)}, \quad (2)$$

where D is damage ($), g is the spatial aggregation unit (e.g., grid cell for distributed analysis, parcel), n is the total number of the flooded spatial units, h is the flood depth, $fc_{g,h}$ is the percent damage (%) corresponding to the flood depth h from the fragility curve for the g^{th} spatial unit, and SV_g is the structural value for the g^{th} spatial unit ($). One U.S. foot (~0.3 m) freeboard was assumed in computing damage since no better information exists to determine the base elevation of a structure [44].

Finally, the annualized risk is calculated as the product of damage and the corresponding flood probability [45]:

$$\boldsymbol{R = D \times P}, \quad (3)$$

where R is the annualized flood risk, and P is the exceedance probability.

As mentioned previously, a definition of spatial aggregation unit and associated monetary value is needed to assess the damage. In this study, the 2011 Snohomish County-assessed parcel dataset

was used to provide the asset value (structural value) for consequence analysis. However, the parcel footprint was not used as the spatial aggregation unit. Rather, an approach was utilized to enhance the spatial resolution of structural representation and avoid estimation of damage in large parcels where the structural footprint is small. To accomplish this, the imperviousness percentages (30 m) from the 2011 U.S. National Land Cover Database was used to filter out the non-developed areas within a parcel. The structural asset value of a given parcel was distributed as a function of imperviousness across the grid cells within the parcel, such that the distributed structural value is conserved when compared to the total parcel value.

3. Results and Discussion

3.1. Precipitation Analysis

Mean-monthly comparisons of precipitation were made to understand the potential cascading bias in the development of local-scale, actionable information. Precipitation from each climate scenario was aggregated to mean-monthly values and compared to the seven weather stations (Table 1). The simulated precipitation of the historic scenario appears to over-predict at stations lower than 100 m, while generally matched well with the observations at higher elevations (Figure 4). While not fully understood, plausible explanations for this variability is that the areas of the lower elevation are subject to local disturbances (e.g. urban impacts, rain-shadow effect), which were not well captured by the RCM. The precipitation curves from both RCP scenarios are consistently higher when compared to historic precipitation, indicating an increasing trend in the precipitation amount projected for the study area. Notably, both RCP scenarios show increased winter precipitation and decreased summer precipitation relative to the historic scenario, a potentially important shift when considering the potential for changes in rain, snow, and rain-on-snow events and preparation for such events.

Preprints (www.preprints.org) | NOT PEER-REVIEWED | Posted: 2 May 2018 doi:10.20944/preprints201805.0044.v1

Peer-reviewed version available at Water 2018, 10, 775; doi:10.3390/w10060775

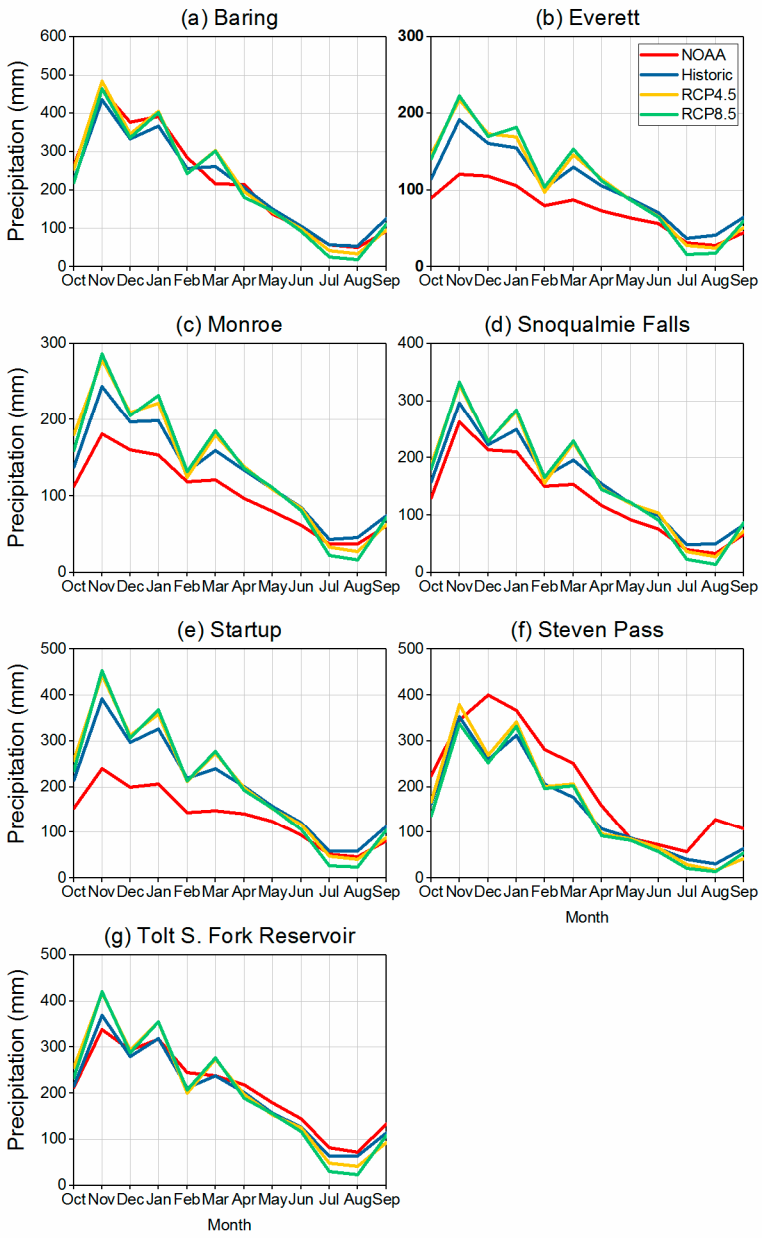

Figure 4. Mean monthly precipitation from seven climate data sets at seven Snohomish watershed locations.

3.2. Streamflow Simulation

The calibrated and validated DHSVM model was used to predict river flow for both climate scenarios and were subsequently compared to the gauged stream flows representing the current condition. To closely examine the potential impact of the temporal shift in precipitation on the timing of annual peak discharge, five occurrences of maximum daily flow were selected for each year in the future period and compared to the gauge observations. For both the RCP4.5 and the RCP8.5 scenarios, there is a clear decrease in the number of months in which peak flows are simulated to occur (Figure 5). That is, there are fewer occurrences of peak flow during the spring and summer months and an increase in the occurrence of peak flows during the winter months. This finding is consistent with the previous observation in this study where projected precipitation extremes tended to shift from spring and summer months to winter months. Comparing the two future scenarios, RCP8.5 scenario tends to have a stronger shift to winter peaks, a potentially important distinction as we compare potential flood risk relative to carbon scenarios.

Preprints (www.preprints.org) | NOT PEER-REVIEWED | Posted: 2 May 2018 doi:10.20944/preprints201805.0044.v1

Peer-reviewed version available at Water 2018, 10, 775; doi:10.3390/w10060775

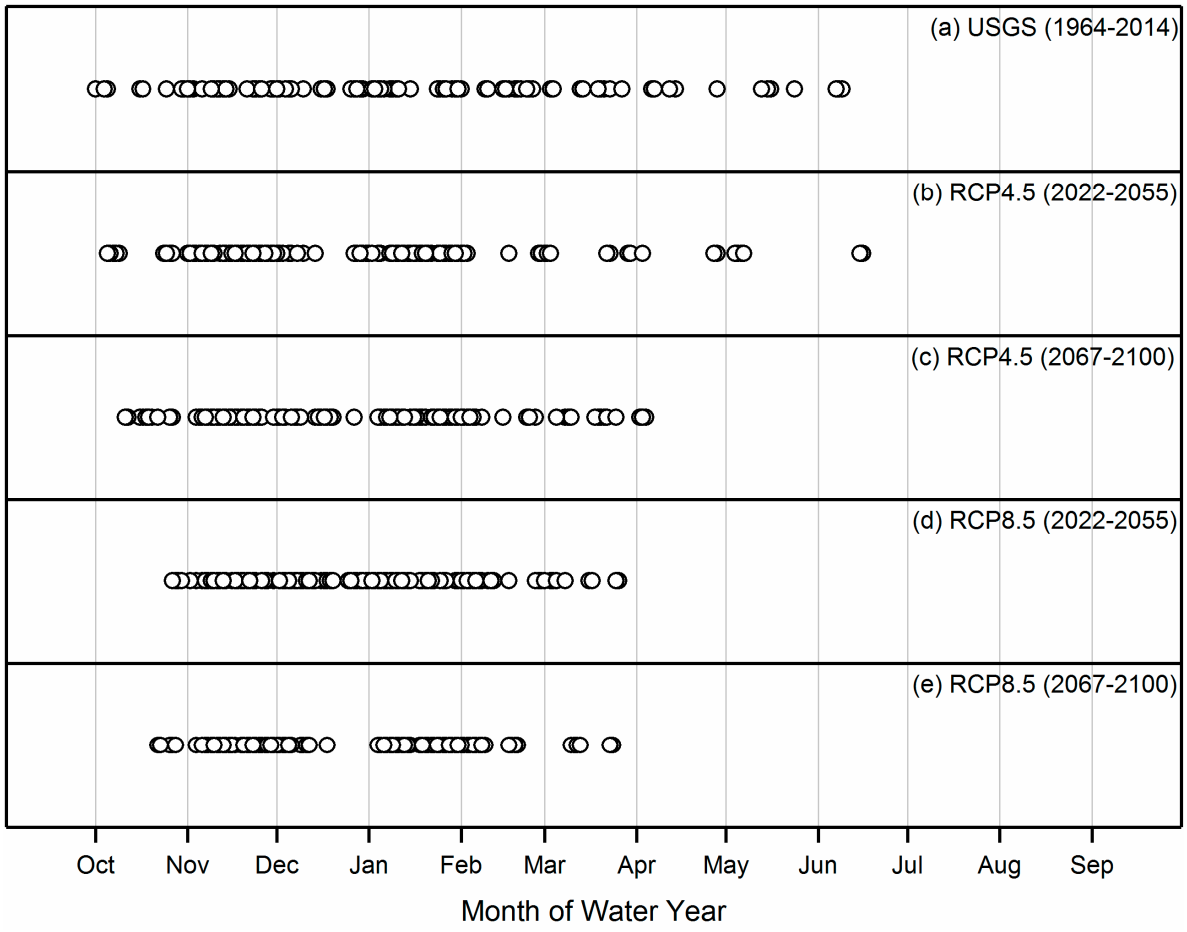

Figure 5. The timing of the five largest daily flows in each water year for different scenarios.

3.3. Streamflow Frequency Analysis

Using the frequency distributions developed using the Bulletin 17C method, direct comparison of annual return period events can be made to quantify relative change in intensity and frequency of extreme flood events. Since traditional frequency analyses such as the Bulletin 17C method implicitly assumed a stationary distribution, each carbon scenario was divided into two time windows. The purpose of this was so as to not dilute future change based on historic conditions. A comparison of the two windows (2022-2055 and 2067-2100), therefore, could directly exhibit the nonstationarity of climate changes (Figure 6). A significant difference between the two future scenarios was found for the period 2022-2055. Compared to RCP4.5, RCP8.5 generally exhibits a smaller increase in peak flows and is especially pronounced for the more extreme return period events, consistent with previous findings [46]. Although the projected peak flows of our RCP8.5 scenario became even slightly lower than the historic conditions for the largest return periods, this was also found by a previous study using 10 GCMs since simulating rare events with the large return periods is always challenging [46] (page 181). Because the occurrence of precipitation peaks and runoff peaks are projected to toward winter months, this finding could be expected to be related to the timing of rain-on-snow events. The potential implications of rain-on-snow events will be discussed in details later.

The later future period (2067-2100) for both scenarios all show an increase in peak river flow when compared to the early future period (2022-2055) (Figure 6). This exposes a nonstationary condition in the magnitude of peak discharges for a given flood probability, and conversely, a nonstationary reduction in the return interval for given peak discharge. These nonstationary changes could be expected to be more intense for the rarer but more severe floods and, therefore, be associated with more significant consequences.

An example can be given to take a closer look at these nonstationary changes. The low end of the return periods is more closely aligned since they were established on a fair amount of historic

Preprints (www.preprints.org) | NOT PEER-REVIEWED | Posted: 2 May 2018 doi:10.20944/preprints201805.0044.v1

Peer-reviewed version available at Water 2018, 10, 775; doi:10.3390/w10060775

events (and therefore more certainty) than the high end of the return periods established based on few, rare events (Figure 6). Among the selected six return periods shown in Figure 7, both climate scenarios projected a larger magnitude of peak flows for a same historic return period. That is, the new 10-year return period in RCP4.5 and RCP8.5 could have more than 9% increase in the peak flows when compared historically. Conversely, the historic 10-year peak flow would be expected to happen, on average, every 5-7 years under both climate scenarios. Even within the selected 200-year time window, the nonstationarity was clearly exhibited with a reverse changing trend between the two periods; i.e. the percent increases in the peak discharges for both RCP4.5 and RCP8.5 scenarios were projected to keep shrinking during 2022-2055 along with the return period, while the percent increase in peak discharges for both scenarios kept enlarging during 2067-2100.

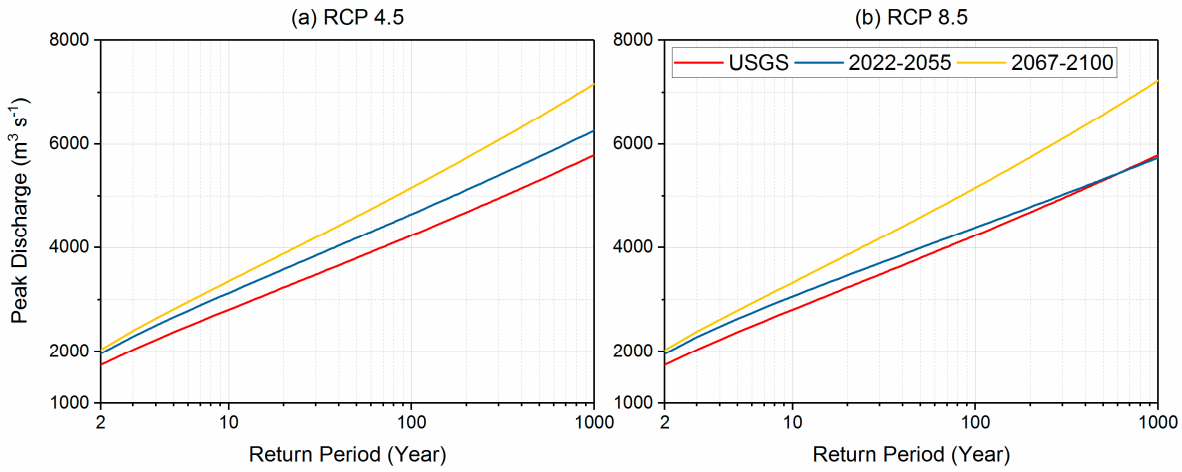

Figure 6. Frequency curves of annual peak flow at Monroe for USGS instantaneous observations (1964-2014), RCP4.5 (a), and RCP8.5 (b) made by the Bulletin 17C method.

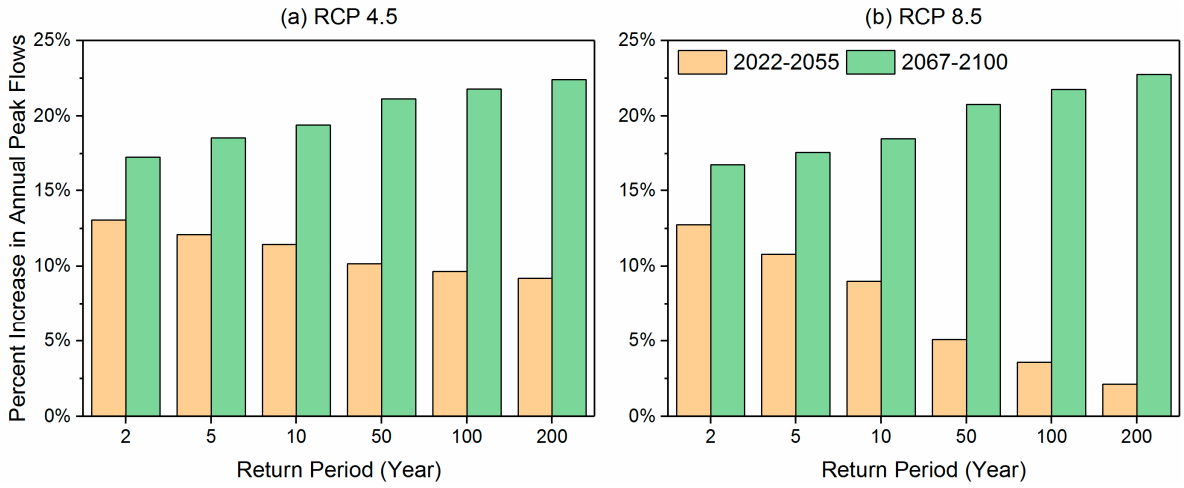

Figure 7. Percent increase of estimated future peak flows for RCP4.5 (a) and RCP8.5 (b) over the historic USGS instantaneous peak flows.

3.4. Peak flows and the role of rain-on-snow events

Given the general perception of increased impacts for more extreme climate scenarios, it may be somewhat non-intuitive to expect the reduced potential for flooding under warmer climate conditions. Peak flows in a river have a complex, nonlinear relationship with precipitation dynamics. Peak flows can be driven by rain events, snowmelt freshets, or rain-on-snow events. To understand the influence of climate scenario of peak flow, snow water equivalent (SWE) (Figure 8) and the prevalence of rain-on-snow conditions (Figure 9) were examined more closely. For rain-on-snow

298 events, changes were quantified by calculating the amount of dime that rain-on-snow events
299 occurred at 5 locations and normalizing each location to the historic period.

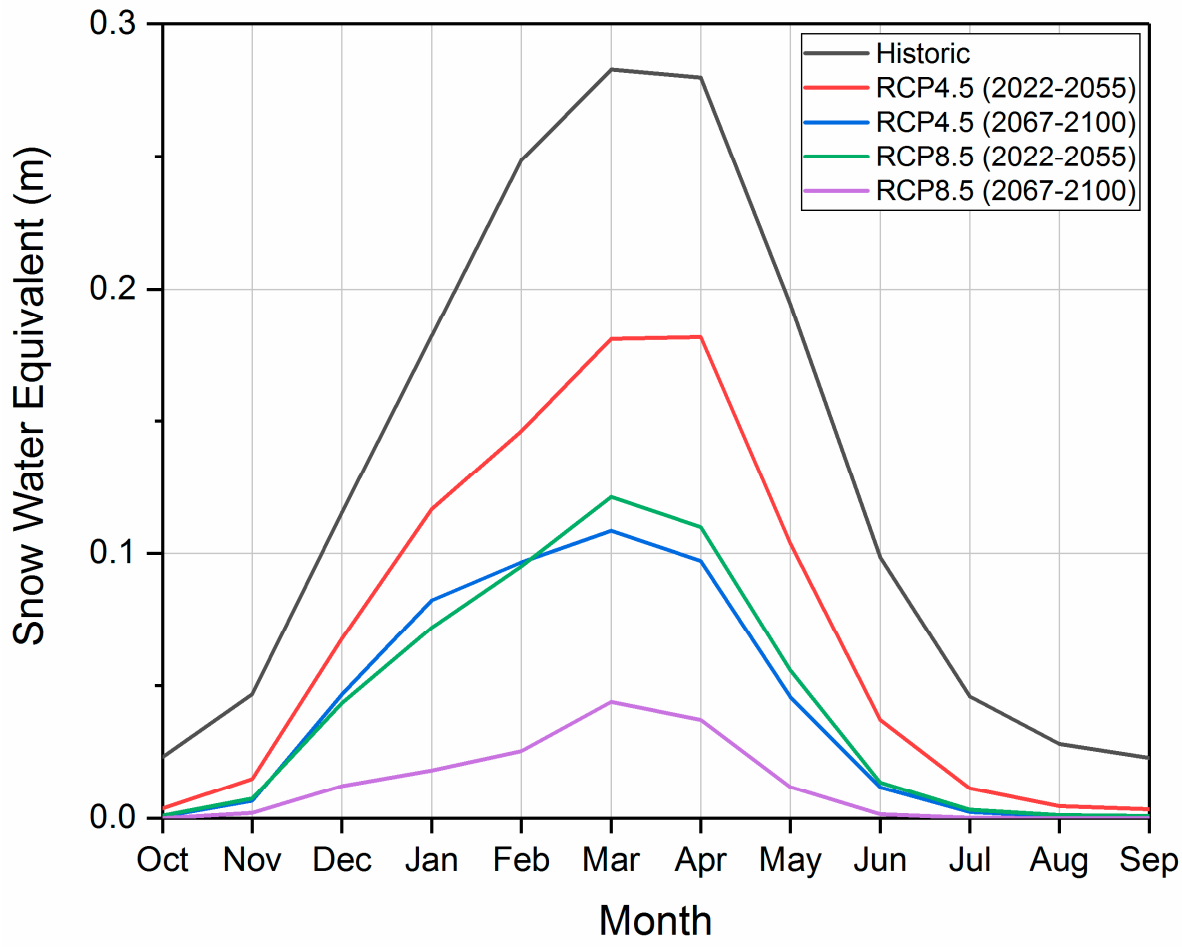

300

301 **Figure 8.** Changes in the basin-wide monthly snow water equivalent.

Preprints (www.preprints.org) | NOT PEER-REVIEWED | Posted: 2 May 2018 doi:10.20944/preprints201805.0044.v1

Peer-reviewed version available at Water 2018, 10, 775; doi:10.3390/w10060775

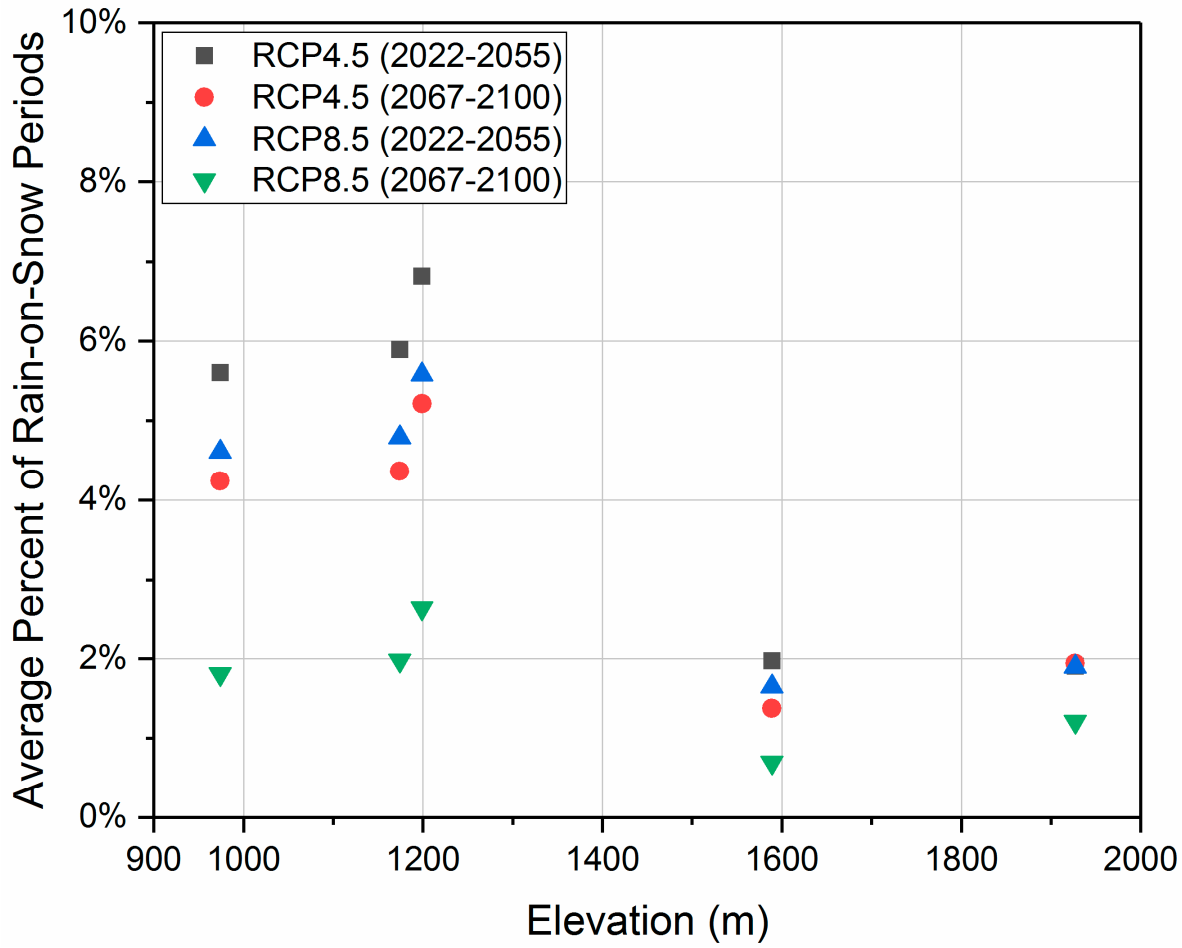

Figure 9. The percent of occurrence of rain-on-snow events occurred at 5 randomly selected elevations.

Relative to the historic scenario, all RCP pathways had a decreased snow water equivalent (SWE), which means a larger fraction of the precipitation fell as rain. Considering that the precipitation peaks were projected to shift more towards winter months, more rain and rain-on-snow events were projected to happen considering an increase in temperature. This would tend to reduce snowmelt-driven peak flows in the springtime but trigger more intensive rain and rain-on-snow driven peak flow events. However, both time periods of the RCP8.5 scenario exhibited less SWE than RCP4.5 (Figure 8), indicating a more intensive reduction in the snowpack and reducing the potential for rain-on-snow occasions in the RCP8.5. Particularly, the second period (2067-2100) of RCP8.5 had the least amount of snowpack (Figure 8) and the least occurrence of rain-on-snow events (Figure 9) due to increase in temperature in which case the snowpack may melt before being compounded with the upcoming winter storms. This could explain why the second period of RCP8.5 had larger peak flows (Figure 6), which would be only in response to rainfall as found by Madsen et al [47].

Surprisingly, the first period (2022-2055) of RCP8.5 had the moderate amount of remaining SWE (Figure 8) and frequent rain-on-snow events (Figure 9) but the reduced peak-flow magnitudes (Figure 6), which was also found by multiple previous studies as summarized by Madsen et al [47]. The reason for these similar declined flood magnitudes is still not clear, but they should be related to the timing and the conversion between rain and snow.

3.5. Quantification of Consequences

The end products of the integrated multi-scale, multi-model framework quantify the flood risk at a local scale. In this case, only the later time period is considered when evaluating future flood risk. The frequency distribution for the two climate scenarios for the later time period is shown in Figure 10. RCP8.5 had a frequency distribution with peak discharges that were less than the discharges in

Preprints (www.preprints.org) | NOT PEER-REVIEWED | Posted: 2 May 2018 doi:10.20944/preprints201805.0044.v1

Peer-reviewed version available at Water 2018, 10, 775; doi:10.3390/w10060775

RCP4.5. Therefore, RCP4.5 represents the more severe flow condition in this study case, while RCP8.5 would fall within the envelope bounded by USGS and RCP4.5.

To capture the most extreme chance for change under future climate scenarios, only the USGS (used as a baseline) and RCP4.5 frequency distributions were used. Due to the projected climate change (from USGS to RCP4.5), the studied watershed would experience 24%, 33%, 29% increases in both damage and annualized risk (with the same rates) for the 10-year, 100-year, and 1000-year floods (Figure 11). The maximum annualized flood risk was raised by 15% from the USGS condition to RCP4.5 condition, while both of the maximums occurred at the 1.2-year flood, indicating that the mitigation measures should most target the repetitive low-risk floods for this region. The damage caused by the historic 10-year flood would be expected to be equivalent to damage of the new 5-year flood in the projected future climate, while the damage caused by the historic 100-year flood would be projected to the only amount to the damage of the new 29-year flood. This indicates the necessity to incorporate the climate change into the strategic planning to manage the future flood management.

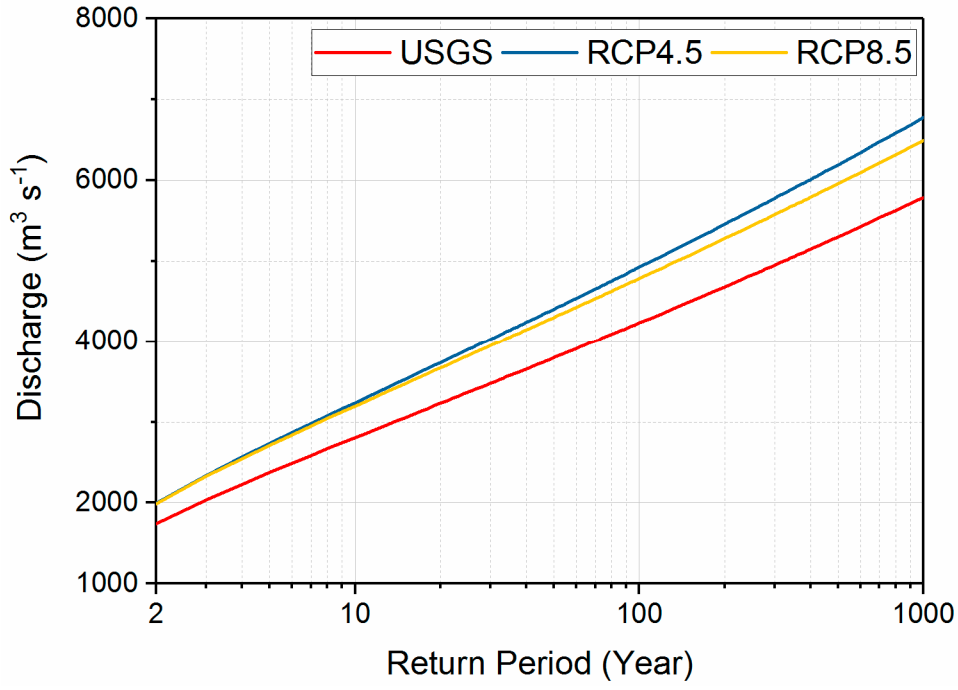

Figure 10. Frequency curves of annual peak flow with combined two periods for USGS instantaneous observations, RCP4.5 (a), and RCP8.5 (b) made by the Bulletin 17C method.

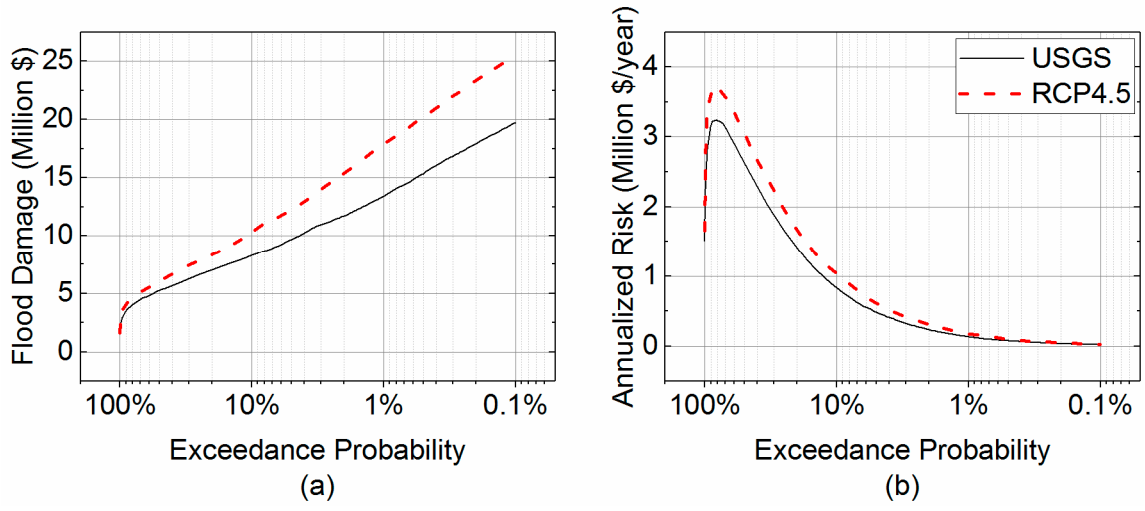

Figure 11. The damage (a) and annualized risk (b) of USGS and RCP4.5 flow conditions.

4. Conclusions

The primary outcome of this project is the demonstration of the ability to utilize regional-scale climate data to develop local-scale runoff distributions that can be used for community and infrastructure planning. While the focus of this project was extreme precipitation and runoff relative to flooding, the same approach can be utilized to investigate water management strategies relative to temporal shifts in annual runoff volume under water-stressed conditions.

Major findings of this study can be summarized as follows.

(1) The peak flows simulated by the proposed model chain have been calibrated and validated by compared to the observation;
(2) The peaks of precipitation and streamflows were projected to shift from spring and summer to the earlier winter season;
(3) The nonstationarity of peak discharges was exhibited from both RCP4.5 and RCP8.5 scenarios with more frequent and severe flood risks projected in the longer future.
(4) The RCP 4.5 pathway projected overall higher peak flows than the RCP 8.5 pathway for the study region, where more rain-on-snow events projected by RCP4.5 might be the reason.

Acknowledgments: This work was mainly sponsored by Pacific Northwest National Laboratory (PNNL) Laboratory Directed Research and Development program. PNNL is operated for U.S. Department of Energy by Battelle Memorial Institute under contract DE-AC05-76RL01830. The work also received kind supports from the Snohomish County, WA, U.S.

Author Contributions: D.J. conceived and designed the project; D.J. and C.R. performed the model; S.W., D.J., Y.F., and C.R. analyzed the data; D.J., Y.F., and C.R. wrote the paper. Authorship must be limited to those who have contributed substantially to the work reported.

Conflicts of Interest: The authors declare no conflict of interest.

References

1. Fowler, H.J.; Wilby, R.L. Detecting changes in seasonal precipitation extremes using regional climate model projections: Implications for managing fluvial flood risk. *Water Resources Research*, **2010**. *46*(3).
2. Cheng, L.; AghaKouchak, A. Nonstationary precipitation intensity-duration-frequency curves for infrastructure design in a changing climate. *Scientific reports*, **2014**. *4*: p. 7093.
3. Mailhot, A.; Duchesne, S. Design Criteria of Urban Drainage Infrastructures under Climate Change. *Journal of Water Resources Planning and Management*, **2010**. *136*(2): p. 201-208.
4. Kim, B.S.; Kim, B.K.; Kwon, H.H. Assessment of the impact of climate change on the flow regime of the Han River basin using indicators of hydrologic alteration. *Hydrological Processes*, **2011**. *25*(5): p. 691-704.
5. Wood, A.W.; Leung, L.R.; Sridhar, V.; Lettenmaier, D.P. Hydrologic Implications of Dynamical and Statistical Approaches to Downscaling Climate Model Outputs. *Climatic Change*, **2004**. *62*(1): p. 189-216.
6. Prudhomme, C.; Jakob, D.; Svensson, C. Uncertainty and climate change impact on the flood regime of small UK catchments. *Journal of Hydrology*, **2003**. *277*(1-2): p. 1-23.
7. Dulie, V.; Zhang, Y.; Salathe, E.P. Extreme precipitation and temperature over the U.S. Pacific Northwest: A comparison between observations, reanalysis data, and regional models. *Journal of Climate*, **2011**. *24*(7): p. 1950-1964.
8. Fowler, H.J.; Blenkinsop, S.; Tebaldi, C. Linking climate change modelling to impacts studies: recent advances in downscaling techniques for hydrological modelling. *International Journal of Climatology*, **2007**. *27*(12): p. 1547-1578.
9. Xu, C.-y. From GCMs to river flow: a review of downscaling methods and hydrologic modelling approaches. *Progress in Physical Geography*, **1999**. *23*(2): p. 229-249.

10. Prudhomme, C.; Reynard, N.; Crooks, S. Downscaling of global climate models for flood frequency analysis: where are we now? *Hydrological Processes*, **2002**. *16*(6): p. 1137-1150.
11. Sunyer, M.A.; Hundecha, Y.; Lawrence, D.; Madsen, H.; Willems, P.; Martinkova, M.; Vormoor, K.; Bürger, G.; Hanel, M.; Kriaučiuniene, J.; Loukas, A.; Osuch, M.; Yücel, I. Inter-comparison of statistical downscaling methods for projection of extreme precipitation in Europe. *Hydrology and Earth System Sciences*, **2015**. *19*(4): p. 1827-1847.
12. Burton, A.; Fowler, H.J.; Blenkinsop, S.; Kilsby, C.G. Downscaling transient climate change using a Neyman-Scott Rectangular Pulses stochastic rainfall model. *Journal of Hydrology*, **2010**. *381*(1-2): p. 18-32.
13. Vormoor, K.; Lawrence, D.; Heistermann, M.; Bronstert, A. Climate change impacts on the seasonality and generation processes of floods - Projections and uncertainties for catchments with mixed snowmelt/rainfall regimes. *Hydrology and Earth System Sciences*, **2015**. *19*(2): p. 913-931.
14. Mizukami, N.; Clark, M.P.; Gutmann, E.D.; Mendoza, P.A.; Newman, A.J.; Nijssen, B.; Livneh, B.; Hay, L.E.; Arnold, J.R.; Brekke, L.D. Implications of the Methodological Choices for Hydrologic Portrayals of Climate Change over the Contiguous United States: Statistically Downscaled Forcing Data and Hydrologic Models. *Journal of Hydrometeorology*, **2016**. *17*(1): p. 73-98.
15. Camici, S.; Brocca, L.; Moramarco, T. Accuracy versus variability of climate projections for flood assessment in central Italy. *Climatic Change*, **2017**: p. 1-14.
16. Khaliq, M.N.; Ouarda, T.B.M.J.; Ondo, J.C.; Gachon, P.; Bobée, B. Frequency analysis of a sequence of dependent and/or non-stationary hydro-meteorological observations: A review. *Journal of Hydrology*, **2006**. *329*(3): p. 534-552.
17. Teng, J.; Jakeman, A.J.; Vaze, J.; Croke, B.F.W.; Dutta, D.; Kim, S. Flood inundation modelling: A review of methods, recent advances and uncertainty analysis. *Environmental Modelling & Software*, **2017**. *90*: p. 201-216.
18. Kalyanapu, A.; Judi, D.; McPherson, T.; Burian, S. Monte Carlo-based flood modelling framework for estimating probability weighted flood risk. *Journal of Flood Risk Management*, **2012**. *5*(1): p. 37-48.
19. Snohomish County. Hazard Mitigation Plan: Summary. 2015.
20. Hamlet, A.F. Assessing water resources adaptive capacity to climate change impacts in the Pacific Northwest Region of North America. *Hydrology and Earth System Sciences*, **2011**. *15*(5): p. 1427-1443.
21. Kraucunas, I.; Clarke, L.; Dirks, J.; Hathaway, J.; Hejazi, M.; Hibbard, K.; Huang, M.; Jin, C.; Kintner-Meyer, M.; van Dam, K.K. Investigating the nexus of climate, energy, water, and land at decision-relevant scales: the Platform for Regional Integrated Modeling and Analysis (PRIMA). *Climatic Change*, **2015**. *129*(3-4): p. 573-588.
22. Gao, Y.; Leung, L.R.; Lu, J.; Liu, Y.; Huang, M.; Qian, Y. Robust spring drying in the southwestern US and seasonal migration of wet/dry patterns in a warmer climate. *Geophysical Research Letters*, **2014**. *41*(5): p. 1745-1751.
23. Skamarock, W.C.; Klemp, J.B.; Dudhia, J.; Gill, D.O.; Barker, D.M.; Duda, M.G.; Huang, X.-y.; Wang, W.; Powers, J.G. A description of the advanced research WRF version 3, in *NCAR Tech. Note*. 2008, Natl. Cent. for Atmos. Res.: Boulder, Colo., U.S.A.
24. Xia, Y.; Mitchell, K.; Ek, M.; Sheffield, J.; Cosgrove, B.; Wood, E.; Luo, L.; Alonge, C.; Wei, H.; Meng, J.; Livneh, B.; Lettenmaier, D.; Koren, V.; Duan, Q.; Mo, K.; Fan, Y.; Mocko, D. Continental-scale water and energy flux analysis and validation for the North American Land Data Assimilation System project phase 2 (NLDAS-2): 1. Intercomparison and application of model products. *Journal of Geophysical Research: Atmospheres*, **2012**. *117*(D3).

25. Hejazi, M.I.; Voisin, N.; Liu, L.; Bramer, L.M.; Fortin, D.C.; Hathaway, J.E.; Huang, M.; Kyle, P.; Leung, L.R.; Li, H.-Y. 21st century United States emissions mitigation could increase water stress more than the climate change it is mitigating. *Proceedings of the National Academy of Sciences*, **2015**. *112*(34): p. 10635-10640.
26. Wigmosta, M.S.; Vail, L.W.; Lettenmaier, D.P. A distributed hydrology-vegetation model for complex terrain. *Water resources research*, **1994**. *30*(6): p. 1665-1679.
27. Yang, Z.; Wang, T.; Voisin, N.; Copping, A. Estuarine response to river flow and sea-level rise under future climate change and human development. *Estuarine, Coastal and Shelf Science*, **2015**. *156*: p. 19-30.
28. Maidment, D.R. Handbook of hydrology. Vol. 1. 1993: McGraw-Hill New York.
29. Yapo, P.O.; Gupta, H.V.; Sorooshian, S. Multi-objective global optimization for hydrologic models. *Journal of hydrology*, **1998**. *204*(1-4): p. 83-97.
30. Moriasi, D.N.; Arnold, J.G.; Van Liew, M.W.; Bingner, R.L.; Harmel, R.D.; Veith, T.L. Model evaluation guidelines for systematic quantification of accuracy in watershed simulations. *Transactions of the ASABE*, **2007**. *50*(3): p. 885-900.
31. England Jr, J.F.; Cohn, T.A.; Faber, B.A.; Stedinger, J.R.; Thomas Jr, W.O.; Veilleux, A.G.; Kiang, J.E.; Mason Jr, R.R. Guidelines for determining flood flow frequency—Bulletin 17C. 2018, US Geological Survey.
32. Brigode, P.; Bernardara, P.; Paquet, E.; Gailhard, J.; Garavaglia, F.; Merz, R.; Micövic̈, Z.; Lawrence, D.; Ribstein, P. Sensitivity analysis of SCHADEX extreme flood estimations to observed hydrometeorological variability. *Water Resources Research*, **2014**. *50*(1): p. 353-370.
33. Qi, W.; Zhang, C.; Fu, G.; Zhou, H.; Liu, J. Quantifying Uncertainties in Extreme Flood Predictions under Climate Change for a Medium-Sized Basin in Northeastern China. *Journal of Hydrometeorology*, **2016**. *17*(12): p. 3099-3112.
34. Hundecha, Y.; Sunyer, M.A.; Lawrence, D.; Madsen, H.; Willems, P.; Bürger, G.; Kriaučiūnienė, J.; Loukas, A.; Martinkova, M.; Osuch, M.; Vasiliades, L.; von Christierson, B.; Vormoor, K.; Yücel, I. Inter-comparison of statistical downscaling methods for projection of extreme flow indices across Europe. *Journal of Hydrology*, **2016**. *541, Part B*: p. 1273-1286.
35. Jiang, P.; Gautam, M.R.; Zhu, J.; Yu, Z. How well do the GCMs/RCMs capture the multi-scale temporal variability of precipitation in the Southwestern United States? *Journal of Hydrology*, **2013**. *479*: p. 75-85.
36. Camici, S.; Brocca, L.; Melone, F.; Moramarco, T. Impact of climate change on flood frequency using different climate models and downscaling approaches. *Journal of Hydrologic Engineering*, **2014**. *19*(8).
37. Condon, L.E.; Gangopadhyay, S.; Pruitt, T. Climate change and non-stationary flood risk for the upper Truckee River basin. *Hydrology and Earth System Sciences*, **2015**. *19*(1): p. 159-175.
38. Seidou, O.; Ramsay, A.; Nistor, I. Climate change impacts on extreme floods I: Combining imperfect deterministic simulations and non-stationary frequency analysis. *Natural Hazards*, **2012**. *61*(2): p. 647-659.
39. Kourgialas, N.N.; Dokou, Z.; Karatzas, G.P. Statistical analysis and ANN modeling for predicting hydrological extremes under climate change scenarios: The example of a small Mediterranean agro-watershed. *Journal of Environmental Management*, **2015**. *154*: p. 86-101.
40. Jaw, T.; Li, J.; Hsu, K.L.; Sorooshian, S.; Driouech, F. Evaluation for Moroccan dynamically downscaled precipitation from GCM CHAM5 and its regional hydrologic response. *Journal of Hydrology: Regional Studies*, **2015**. *3*: p. 359-378.
41. Lu, Y.; Qin, X.S.; Xie, Y.J. An integrated statistical and data-driven framework for supporting flood risk analysis under climate change. *Journal of Hydrology*, **2016**. *533*: p. 28-39.
42. Judi, D.R.; Burian, S.J.; McPherson, T.N. Two-dimensional fast-response flood modeling: Desktop parallel computing and domain tracking. *Journal of Computing in Civil Engineering*, **2010**. *25*(3): p. 184-191.

43. Scawthorn, C.; Flores, P.; Blais, N.; Seligson, H.; Tate, E.; Chang, S.; Mifflin, E.; Thomas, W.; Murphy, J.; Jones, C.; Lawrence, M. HAZUS-MH Flood Loss Estimation Methodology. II. Damage and Loss Assessment. *Natural Hazards Review*, **2006**. *7*(2): p. 72-81.

44. FEMA. Technical Bulletin 10: Ensuring that structures built on fill in or near special flood hazard areas are reasonably safe from flooding. 2001.

45. Kalyanapu, A.J.; Judi, D.R.; McPherson, T.N.; Burian, S.J. Annualised risk analysis approach to recommend appropriate level of flood control: application to Swannanoa river watershed. *Journal of Flood Risk Management*, **2015**. *8*(4): p. 368-385.

46. Snohomish County. Hazard Mitigation Plan: Volume 1 Risk Assessment. 2015.

47. Madsen, H.; Lawrence, D.; Lang, M.; Martinkova, M.; Kjeldsen, T.R. Review of trend analysis and climate change projections of extreme precipitation and floods in Europe. *Journal of Hydrology*, **2014**. *519*: p. 3634-3650.